THE JOURNAL OF PHYSICAL CHEMISTRY Letters

Letter

pubs.acs.org/JPCL

Ring Polymer Surface Hopping: Incorporating Nuclear Quantum Effects into Nonadiabatic Molecular Dynamics Simulations

Farnaz A. Shakib* and Pengfei Huo*

Department of Chemistry, University of Rochester, 120 Trustee Road, Rochester, New York 14627, United States

Supporting Information

ABSTRACT: We apply a recently proposed ring polymer surface hopping (RPSH) approach to investigate the real-time nonadiabatic dynamics with explicit nuclear quantum effects. The nonadibatic electronic transitions are described through Tully's fewest-switches surface hopping algorithm and the motion of the nuclei are quantized through the ring polymer Hamiltonian in the extended phase space. Applying the RPSH method to simulate Tully's avoided crossing models, we demonstrate the critical role of the nuclear tunneling effect and zero-point energy for accurately describing the transmission and reflection probabilities with low initial momenta. In addition, in Tully's extended coupling model, we show that the ring polymer quantization effectively captures decoherence, yielding more accurate reflection probabilities. These promising results demonstrate the potential of using RPSH as an accurate and efficient method to incorporate nuclear quantum effects into nonadiabatic dynamics simulations.

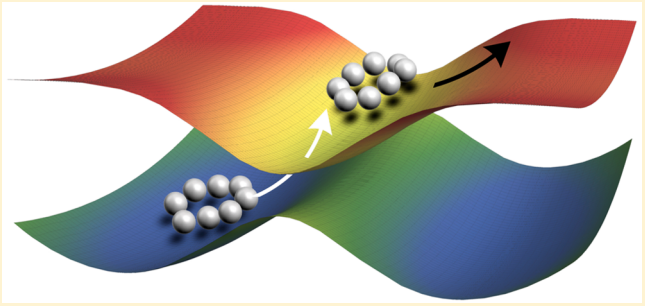

Quantum mechanical effects, such as electronic nonadiabatic transitions and nuclear quantum effects, play an important role in a wide range of chemical reactions. For example, the rate and mechanism of proton-coupled electron transfer (PCET) reactions[1−9] are significantly influenced by these quantum effects. As a result, classical molecular dynamics simulations are not capable of describing such processes. Despite impressive recent progress in numerically exact quantum dynamics methods, simulating these processes in large complex systems remains computationally challenging. The alternative approach is to develop approximated, trajectory-based quantum dynamics methods that are capable of accurately describing these quantum effects.

Electronic nonadiabatic effects have been successfully incorporated in the mixed quantum−classical approaches, including Ehrenfest dynamics,[10−12] fewest-switches surface hopping (FSSH),[13,14] and mixed quantum−classical Liouville dynamics (MQCL).[15,16] Continuous efforts are also being made on incorporating these effects into the semiclassical initial value representation (SC-IVR)[17] and its linearized versions.[18−23] FSSH turned out to be one of the most widely used methods[24−26] because it is computationally efficient and conceptually simple,[13] representing a quantum wavepacket with an ensemble of independent classical trajectories. The classical trajectories are propagated on one single adiabatic surface, except instantaneous nonadiabatic transitions (hops) to the other surfaces based on the fewest-switches criterion.[13] The probability of hopping is determined with the quantum amplitudes obtained from the time-dependent Shrödinger equation along the motion of the classical trajectories.[13]

Despite the success of FSSH in studying nonadiabatic dynamics, it has well-known shortcomings.[25,26] First, the classical trajectories can not properly describe nuclear quantum effects such as nuclear tunneling and zero-point energy (ZPE). Second, FSSH suffers from neglecting decoherence.[27−31] Although there have been a considerable number of attempts to resolve these shortcomings,[31−38] the classical trajectories used in these methods still hamper the accurate description of quantum dynamics when nuclear quantum effects play an important role.

Imaginary-time path-integral approaches, including centroid molecular dynamics (CMD)[39,40] and ring polymer molecular dynamics (RPMD),[41] have been successfully developed and applied to investigate nuclear quantum effects and electronic nonadiabatic dynamics in large-scale condensed-phase simulations.[42] In these methods, nuclear quantum effects are captured with the Feynman's imaginary-time path-integral formalism, leading to a ring polymer classical isomorphism that describes ZPE and tunneling effects in the extended classical phase space.[42] Despite its success in describing quantum effects in the condensed phase, the regular RPMD approach is limited to one-electron nonadiabatic dynamics or nuclear quantization,[5,42] as well as the lack of the real-time electronic coherence effects.[42,43] To address these challenges, recent efforts have been focused on developing CMD[44] and RPMD approaches with the many-electronic-states representation.[45−50]

Among the recently developed state-dependent RPMD approaches, ring polymer surface hopping (RPSH)[45,51] is one

Received: May 29, 2017
Accepted: June 20, 2017
Published: June 20, 2017

DOI: 10.1021/acs.jpclett.7b01343
J. Phys. Chem. Lett. 2017, 8, 3073−3080

of the potentially promising methods for simulating nonadiabatic dynamics. In RPSH method, the nonadiabatic electronic transitions are described by the FSSH algorithm, and the nuclear quantum effects are incorporated through ring polymer quantization, thus making RPSH a well-tailored theoretical tool for describing the electronic and nuclear quantum dynamics. This method has been demonstrated to give an accurate rate constant for a model barrier crossing problem when nuclear quantization plays an essential role.[45] Hence, we apply the RPSH method[45] to investigate electronic nonadiabatic dynamics in Tully's Model systems with explicit nuclear quantization.

We begin with a brief summary of the RPSH algorithm with the centroid approximation.[45] In this algorithm, the entire ring polymer moves on a single adiabatic state $|\alpha;\mathbf{R}_i\rangle$, with the corresponding Hamiltonian expressed in the extended classical phase space

$$H_n = \sum_{i=1}^{n}\left[\frac{\mathbf{P}_i^2}{2M} + \frac{M}{2}{\omega_n}^2(\mathbf{R}_i - \mathbf{R}_{i-1})^2 + V_\alpha(\mathbf{R}_i)\right] \tag{1}$$

Here, n is the total number of beads, $\omega_n = n/\beta\hbar$, $\beta = 1/k_BT$ is the reciprocal temperature, and $V_\alpha(\mathbf{R}_i) = \langle\alpha;\mathbf{R}_i|\hat{V}|\alpha;\mathbf{R}_i\rangle$ is the potential energy surface (PES) for the adiabatic state $|\alpha;\mathbf{R}_i\rangle$. The corresponding Hamilton's equations of motion for the ring polymer are then expressed as follows

$$\dot{\mathbf{P}}_i = -M{\omega_n}^2(2\mathbf{R}_i - \mathbf{R}_{i-1} - \mathbf{R}_{i+1}) - \frac{\partial V_\alpha(\mathbf{R}_i)}{\partial \mathbf{R}_i}$$

$$\dot{\mathbf{R}}_i = \frac{\mathbf{P}_i}{M} \tag{2}$$

The centroid of the ring polymer position and momentum are defined as

$$\bar{\mathbf{R}} = \frac{1}{n}\sum_{i=1}^{n}\mathbf{R}_i \qquad \bar{\mathbf{P}} = \frac{1}{n}\sum_{i=1}^{n}\mathbf{P}_i \tag{3}$$

and the time-dependent Shrödinger's equation is numerically integrated along the motion of the ring polymer centroid. This gives the electronic coefficients c_α associated with each adiabatic state based on the following equation

$$i\hbar\dot{c}_\alpha(t) = V_\alpha(\bar{\mathbf{R}})c_\alpha(t) - i\hbar\sum_\gamma \dot{\bar{\mathbf{R}}}\cdot\mathbf{d}_{\alpha\gamma}(\bar{\mathbf{R}})c_\gamma(t) \tag{4}$$

From now on, we use the atomic units such that $\hbar = 1$. The energy of the adiabatic state $V_\alpha(\bar{\mathbf{R}}) = \langle\alpha;\bar{\mathbf{R}}|\hat{V}|\alpha;\bar{\mathbf{R}}\rangle$ depends on the centroid position $\bar{\mathbf{R}}$, and the nonadiabatic coupling vector between the two adiabatic states α and γ is

$$\mathbf{d}_{\alpha\gamma}(\bar{\mathbf{R}}) = \langle\alpha;\ \bar{\mathbf{R}}|\nabla_{\bar{\mathbf{R}}}|\gamma;\ \bar{\mathbf{R}}\rangle \tag{5}$$

According to the "fewest-switches" algorithm, the probability of switching from the current state α to all of the other states γ during the time interval between t and $t + \delta t$ is

$$g_{\alpha\gamma} = \frac{-2\mathrm{Re}(\rho_{\gamma\alpha}^*\dot{\bar{\mathbf{R}}}\cdot\mathbf{d}_{\gamma\alpha}(\bar{\mathbf{R}}))\delta t}{\rho_{\alpha\alpha}} \tag{6}$$

where $\rho_{\alpha\gamma} = c_\alpha c_\gamma^*$ is the electronic density matrix element. The nonadiabatic transition, that is, the stochastic switch to any other state γ, is determined by comparing $g_{\alpha\gamma}$ to a randomly generated number between 0 and 1. The transition occurs if the probability flux $g_{\alpha\gamma}$ is greater than the random number.

If a transition occurs, the entire ring polymer hops to the new adiabatic state γ, while the velocity of each bead in the ring polymer is rescaled along the direction of the centroid nonadiabatc coupling vector $\mathbf{d}_{\alpha\gamma}(\bar{\mathbf{R}})$ in order to conserve energy

$$\dot{\mathbf{R}}_i' = \dot{\mathbf{R}}_i - \lambda_{\alpha\gamma}\mathbf{d}_{\alpha\gamma}(\bar{\mathbf{R}})/M \tag{7}$$

The universal scaling constant $\lambda_{\alpha\gamma}$ is calculated with the smallest magnitude obtained from the following expression[14,52]

$$\lambda_{\alpha\gamma} = \frac{1}{a_{\alpha\gamma}}[b_{\alpha\gamma} \pm \sqrt{{b_{\alpha\gamma}}^2 + 2a_{\alpha\gamma}c_{\alpha\gamma}}] \tag{8}$$

where $a_{\alpha\gamma} = {\mathbf{d}_{\alpha\gamma}}^2(\bar{\mathbf{R}})/M$, $b_{\alpha\gamma} = \dot{\bar{\mathbf{R}}}\cdot\mathbf{d}_{\alpha\gamma}(\bar{\mathbf{R}})$, and $c_{\alpha\gamma} = V_\alpha(\bar{\mathbf{R}}) - V_\gamma(\bar{\mathbf{R}})$. It should be noted that this velocity algorithm conserves the energy at the centroid level, and the results presented in this Letter were obtained with this algorithm. Alternatively, one can conserve the energy for the entire ring polymer[45] using $c_{\alpha\gamma} = \frac{1}{n}\sum_i V_\alpha(\mathbf{R_i}) - \frac{1}{n}\sum_i V_\gamma(\mathbf{R_i})$. Additional results for velocity rescaling based on ring polymer energy conservation are presented in the Supporting Information.

The nonadiabatic transition (hop) will be rejected if there is not enough kinetic energy to compensate for the change of potential energy, and then the ring polymer will continue to evolve on the adiabatic state α without any velocity reversal procedure.[53]

We emphasize that in the one-bead or high-temperature limit, RPSH reduces back to the original FSSH, which accurately captures the electronic nonadiabatic transitions in most of the scenarios. On the other hand, in the limit of adiabatic reactions, RPSH reduces back to the conventional RPMD method, which is capable of capturing nuclear quantum effects. Thus, RPSH is a promising method for studying processes that are highly impacted by the interplay between nonadiabatic and nuclear quantum effects, such as PCET reactions.[3,5,7]

To investigate the capability of the RPSH method for describing nonadabatic dynamics, we compute the branching probabilities with Tully's Models I–III in the original FSSH paper.[13] Additional results are also obtained from the FSSH as well as the numerical exact split-operator Fourier transform method in order to compare and assess the accuracy of RPSH.

The initial wave function for all three model calculations is a Gaussian wavepacket on the lower electronic adiabatic surface with the following form

$$G(R) = \left(\frac{2\alpha}{\pi}\right)^{1/4}\exp(-\alpha(R - R_0)^2 + ik(R - R_0)) \tag{9}$$

Here, the width of the wavepacket is $\alpha = 0.25$ au, and $R_0 = -15$ au, ensuring that the initial wavepacket is far from the nonadiabatic coupling region; the nuclear mass is $M = 2000$ au, and k is the incoming momentum. In FSSH and RPSH calculations, this wave function is represented with a Gaussian distribution of nuclear position with the width $\sigma_R = 1/\sqrt{2\alpha}$.[33] For results at each k, the calculations start with a distribution of the initial position around R_0 and a deterministic momentum[13,33] for both FSSH and PRSH methods, ensuring a fair comparison. The choice of the deterministic momentum for the initial condition[33,54] allows us to investigate the role of nuclear quantization without any impact from initial momentum distribution.

To make sure that ring polymer quantization during dynamical propagation plays an essential role for recovering

DOI: 10.1021/acs.jpclett.7b01343
J. Phys. Chem. Lett. 2017, 8, 3073–3080

correct quantum scattering probabilities, we also perform FSSH calculations with the same initial distribution of the centroid in RPSH, as well as with an initial distribution sampled from the Wigner transformed wavepacket in eq 9. These results, provided in the Supporting Information, emphasize that including nuclear quantization through RPMD is indeed the key for improving the transmission and reflection probabilities and cannot be attributed only to the initial conditions of the trajectories.

In addition, we want to comment on a widely used procedure that samples the Wigner initial distribution for FSSH calculations.[55,56] The Wigner initial distribution can indeed improve FSSH results in certain special cases, such as the low-momentum regime in Tully's Model I.[56] However, it does not always guarantee to improve the results, such as in Tully's Model II. Additional results that demonstrate this point are presented in Figure S3 of the Supporting Information. On top of that, we also want to emphasize that in practical simulations, using Wigner distributions can bring additional technical difficulties. First, Wigner distribution is difficult to compute for complex systems.[57−59] Second, a classical propagation scheme does not preserve the Wigner distribution[60] and might lead to a ZPE leaking problem.[61] On the other hand, incorporating nuclear quantization through dynamical propagation of the ring polymer provides consistent improvement of the results, as will be demonstrated later, as well as a practical way to avoid nontrivial quantum distribution calculations and ZPE leaking problems.[61]

The RPSH Hamiltonian requires a temperature for propagating quantum dynamics. For the model calculations under microcanonical conditions in this study, we choose a fictitious temperature that matches the total initial energy of the system through $T = \hbar k/k_B$, based on the procedure outlined in a previous study using MV-RPMD.[49] Despite this ad hoc choice, it is shown that this fictitious temperature can provide accurate results for photoinitiated dynamics.[49] Further theoretical justification is necessary. However, we do not expect it to become an issue for any real system with a physical temperature, which will be used in the RPSH calculations.

The converged results are obtained with 20000 trajectories in both FSSH and RPSH methods. The bead convergence criterion for RPSH calculations is set to be the convergence of the long-time adiabatic populations. For Model I, $n = 4$ beads will converge the results, for Model II, $n = 8$ beads, and for Model III, depending on the initial momentum, up to 32 beads are needed. Examples of the convergence with respect to the number of beads are provided in the Supporting Information.

Figure 1 presents the branching probabilities as a function of the initial momentum k for Tully's Model I, a single avoided crossing model with FSSH, RPSH, and the numerical exact method. Here, Figure 1a presents the results of transmission probabilities T1 (on lower surface) and T2 (on upper surface) as well as reflection probability R1 (on lower surface) for three different parameter regions, with $k = 2-6.5$, 6.5−10, and 10−60 au. Reflection on the upper state R2 is omitted in this plot for clarity purposes due to its zero value for all three methods. In the third region where $k = 10-60$ au, the incoming momentum is high, and the electronic nonadiabatic dynamics between the lower and upper adiabatic surfaces can be well captured by using classical trajectories. Both FSSH and RPSH reproduce the numerical exact results, similar to most of the mixed quantum−classical methods. Thus, we shall only focus on the first two regions where the incoming momentum is low.

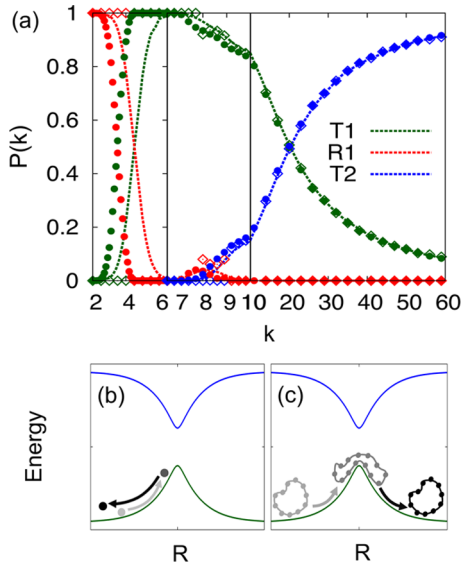

Figure 1. (a) Branching probabilities as a function of the initial momentum k for Model I with FSSH (open diamond), RPSH (filled circle), and the numerical exact method (dashed lines). (b) Schematic trajectory of FSSH in the region of $k = 2-6.5$. (c) Schematic trajectory of RPSH in the same region.

In the first region of Figure 1a where $k = 2-6.5$, the incoming momentum is so low that the scattering process occurs adiabatically. The exact results show that in this regime the wavepacket either gets transmitted (T1) or reflected (R1) on the lower adiabatic surface, with the relative magnitudes of T1 and R1 being determined by the quantum mechanical tunneling process at the given incoming momentum k. FSSH or any other classical trajectory-based method fails to accurately describe the smooth transition between T1 and R1 when using the deterministic initial momentum for the ensemble of trajectories.[33,56] Instead, FSSH (in this case, classical adiabatic dynamics) predicts 100% reflection whenever the trajectories do not have enough kinetic energy to surmount the energy barrier. This limitation is schematically illustrated in Figure 1b where a classical trajectory does not have enough momentum to reach the energy barrier top and thus gets reflected. After $k = 4.5$, however, the classical trajectories have enough kinetic energy to cross the lower adiabatic potential barrier, leading to 100% transmission and a sudden switch of the T1 and R1 coefficients.

RPSH, which is reduced to the adiabatic RPMD in this low-momentum region, incorporates nuclear quantum effects through the extended ring polymer phase space and correctly describes quantum tunneling through the barrier. Thus, RPSH recovers the correct physical behavior in this regime and captures the trend of the smooth transition between R1 and T1, despite small quantitative differences with the numerical exact results. The schematic representation in Figure 1c shows that the ring polymer spans over the top of the ground-state adiabatic potential and effectively reduces the energy barrier. This allows the ring polymer to manifest the quantum mechanical tunneling behavior. In fact, it is well-known that RPMD can successfully describe quantum tunneling dynamics in this electronically adiabatic regime.[62,63] However, this is a challenging regime for the mixed quantum−classical methods due to the classical description of the trajectories.

DOI: 10.1021/acs.jpclett.7b01343
J. Phys. Chem. Lett. 2017, 8, 3073−3080

Figure 2 presents a magnified branching probabilities plot that corresponds to the second region of Figure 1, where k =

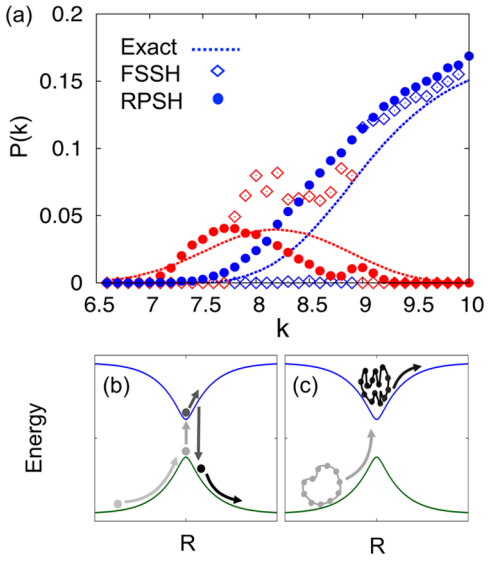

Figure 2. (a) Magnified plot of branching probabilities R1 (red) and T2 (blue) for Model I with incoming momentum k = 6.5−10 with FSSH (open diamond), RPSH (filled circle), and the numerical exact method (dashed lines). (b) Schematic trajectory of FSSH in the region of k = 6.5−10. (c) Schematic trajectory of RPSH in the same region.

6.5−10 au. In this region, the interplay between nuclear quantum effects and electronic nonadiabatic transitions has an important role in determining the quantum dynamics. The exact results (dash lines) in Figure 2a show a small increase and then decrease of R1 (red) and a steady increase of T2 (blue) in this region. This behavior is due to the fact that with low incoming momentum and after nonadiabatic transition to the upper surface, the wavepacket gets trapped in the upper potential well and finally comes down to the lower surface, bifurcating to reflecting and transmitting wavepackets, thus leading to an initially increased R1 in this region.[33] However, as the incoming momentum increases, the wavepacket will escape from this well and remain transmitted on the upper surface, leading to a smooth increase of T2 (blue) at the expense of the decrease in T1 (green in Figure 1) and R1 (red).

FSSH (open diamonds in Figure 2), fails to reproduce these results. In the region of k < 7.7, the classical trajectories do not have enough kinetic energy to jump to the upper adiabatic surface, leading to 100% transmission on the lower surface without any reflection, contradictory to what the exact quantum dynamics predicts. In the region of 7.7 < k < 8.9, classical trajectories have enough kinetic energy to jump to the upper adiabatic surface but not enough to climb out of the potential well on that surface, leading to transitions back to the lower surface, as indicated by the schematic illustration in Figure 2b. Consequently, we find a sudden increase of R1 (red) from 0 to a finite value accompanied by a similar sudden decrease of T1 (shown in the Supporting Information) at k = 7.7. In the region of k > 8.9, the classical trajectories are able to climb out of the upper adiabatic potential well, leading to a stark increase of T2 (blue) from 0 to a finite value, which is in contrast to the smooth increase of T2 predicted by the quantum exact results.

RPSH (filled circles in Figure 2), on the other hand, captures the smooth increase of R1 (red) in the region of k < 7.7 due to the higher kinetic energy of the ring polymer centroid compared to the classical trajectory. Just like the situation in the exact calculations, the ring polymer successfully hops to the upper surface but gets trapped in the upper potential well and later hops back to the lower surface getting either reflected or transmitted. In the region of 7.7 < k < 8.9, RPSH recovers the correct quantum behavior by capturing ZPE in the upper surface, effectively filling the potential well and allowing the ring polymer to escape, as indicated by the schematic illustration in Figure 2c. Thus, in this region, RPSH recovers the smooth increase of T2 (blue). Like the exact results, the increasing trend of T2 in RPSH smoothly continues to the region of k > 8.9.

Figure 3 presents the results for Tully's Model II, a dual avoided crossings model. The branching probabilities of Model

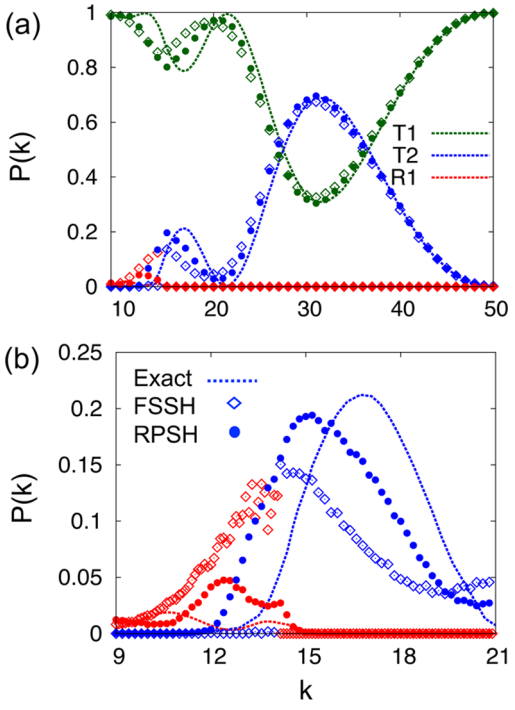

Figure 3. (a) Branching probabilities as a function of the initial momentum k for Model II, with FSSH (open diamond), RPSH (filled circle), and the numerical exact method (dashed lines). (b) Magnified plot for T2 and R1 in the low-momentum regime with k = 9.0−21 au.

II are illustrated in Figure 3a, with a magnified plot of k = 9.0−21 au region in Figure 3b. As can be seen, at high momenta, where k > 21 au, both FSSH and RPSH yield results close to the exact ones, though RPSH seems to produce slightly better results. In the region of k = 9.0−21 au, on the other hand, capturing the nuclear quantum effects is essential for accurately describing nonadiabatic dynamics.

Figure 3b presents the results with the incoming momentum of k = 9.0−21 au. In the region of k = 9.0−12 au, the numerical exact calculations suggest that the dynamics is purely adiabatic where the wavepacket mainly crosses the potential well on the lower surface and gets transmitted. This leads to a near unity T1 (green lines in Figure 3a) and a very small magnitude of the reflection coefficient R1 (red lines in Figure 3b) on the lower surface. In the region of k = 12−21 au, apart from a negligible amount of R1, the wavepacket gets transmitted either on the lower or on the upper surfaces, with the relative magnitude of

DOI: 10.1021/acs.jpclett.7b01343
J. Phys. Chem. Lett. 2017, 8, 3073−3080

T1 (green lines in Figure 3a) and T2 (blue lines in Figure 3a) being determined by quantum mechanical effects.

FSSH results in Figure 3, in contrast, show a steady increase of R1 in the region of k = 9.0−12 au (adiabatic regime), significantly overestimating the reflection probability compared to the numerical exact results. The increase of the FSSH-calculated R1 continues beyond k = 12 au until a sudden decrease to zero at k = 14.2 au, being replaced by a finite value of T2. This behavior indicates that before k = 14.2 au the classical trajectories that jump to the upper surface get trapped there and finally come down to the lower state, being either reflected or transmitted. Beyond k = 14.2, the trajectories have enough kinetic energy to climb out of the upper potential well and get transmitted on that surface. These results clearly demonstrate that FSSH fails to capture the gradual increasing and then decreasing feature of the T2 in the region of k = 12−21 au predicted by exact quantum dynamics.[34]

RPSH, on the other hand, yields smaller values of R1 in the adiabatic regime (k = 9.0−12 au) and, at the same time, captures a similar trend of the changes of R1 and T2 in the region of k = 12−21 au compared to exact results. The improved results of RPSH compared to FSSH can be mainly related to enforcing ZPE through the extended ring polymer phase space. This results in a shallower potential well on the lower surface of Tully's Model II, which helps the transmission of RPSH trajectories in the region of k = 9.0−12 au, leading to a higher T1 and lower R1 compared to FSSH results. Further, ring polymer quantization also helps with transmission on the upper surface in the region of k = 12−21 au, improving T2 coefficients. Similar improvements were also reported by using the Liouville space FSSH (LS-FSSH) method[38] that benefits from propagating classical trajectories on coherent surfaces $\frac{1}{2}(V_1 + V_2)$.[15] These improvements have also been observed for both 1D and 2D versions of Tully's Model II using the phase-corrected surface hopping method.[34] On the other hand, simultaneous trajectory surface hopping (STSH)[33] can improve the magnitude of R1 and T2 compared to FSSH but still has the unphysical sudden switch between these two coefficients at k = 14.2 au.

We have also calculated the RPSH branching probabilities for Models I and II with a distribution obtained from the Wigner transformed wavepacket[49] instead of using a deterministic initial momentum.[13,33] The results, provided in the Supporting Information, do not show significant improvements compared to the results based on the deterministic momentum presented in the main text. This emphasizes that incorporating nuclear quantum effects through the dynamical propagation of the ring polymer is the predominant contributing factor for capturing the correct quantum dynamics in the RPSH method, not the initial conditions.

Figure 4 presents the exact, FSSH, and RPSH results for Tully's Model III, a model of extended coupling with reflection. The wavepacket is initially prepared on the far left side of the lower surface. As it travels to the right-hand side of the potential, it goes through a region of high nonadiabatic coupling and gets bifurcated. At low incoming momenta, the wavepacket that moves on the upper surface gets reflected while the wavepacket on the lower surface gets transmitted. The exact results show that the reflected wavepacket on the upper surface gets bifurcated once again upon going through the nonadiabatic coupling region, giving two wavepackets traveling with different momenta on both surfaces. As a result,

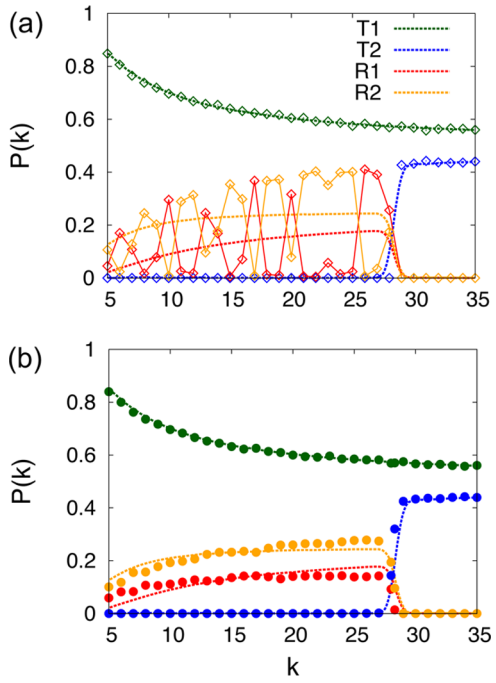

Figure 4. Branching probabilities as a function of the initial k calculated for Model III using (a) FSSH (open diamond) and (b) RPSH (filled circle) methods. The numerical exact results are presented in both panels with dashed lines.

the whole wavepacket experiences a strong decoherence that the FSSH algorithm fails to capture.

FSSH results presented in Figure 4a do not give a smooth change of R1 and R2 coefficients when increasing the incoming momentum; instead, it shows a highly oscillatory behavior due to artificially generated electronic coherence, commonly known as the "over-coherent problem" of FSSH.[13]

Figure 4b demonstrates RPSH branching probabilities for Model III. In contrast to the FSSH method, RPSH yields smooth R1 and R2 that closely follow the exact results, demonstrating the capability of the method to capture decoherence. We emphasize that improvement of reflection probabilities in the RPSH approach is observed using deterministic initial momenta and not a distribution of momenta. In RPSH, due to the extended phase space description of the nucleus through the ring polymer, the momentum of each bead gradually differs through the dynamical propagation, resulting in a broader centroid momentum distribution compared to the distribution in FSSH. Therefore, different reflected ring polymer trajectories gain different phases. Over an ensemble of the ring polymer trajectories, the high-frequency oscillations in reflection coefficients wash out, even with the deterministic initial momenta. These unphysical oscillations can also be removed by introducing decoherence corrections into the surface hopping algorithm, such as the decoherence-induced surface hopping (DISH)[35] method. Similar improvements are also reported using STSH,[33] mean-field surface hopping,[27] and augmented FSSH (A-FSSH)[31] algorithms.

The time-dependent electronic state populations can also be reliably obtained from RPSH. In the Supporting Information, we provide the time-dependent adiabatic and diabatic populations. With nuclear quantization, RPSH is not only capable of capturing long-time scattering probabilities but also

DOI: 10.1021/acs.jpclett.7b01343
J. Phys. Chem. Lett. 2017, 8, 3073−3080

shows an improved short-time population compared to FSSH. Further, with a three-state Morse potential model calculation, we demonstrate a more stable bead convergence for the population dynamics compared to the previously developed state-dependent RPMD method.[49]

Recent theoretical progress suggests that RPMD can be rigorously derived from Matsubara dynamics with a generalized kubo-transformed time correlation function formalism.[64,65] In addition, surface hoping has also been mathematically derived from the mixed quantum−classical Liouville equation.[16,66] We thus envision deriving RPSH in the nonadiabatic Matsubara dynamics framework[67] with MQCL[16] as one of our future goals.

RPSH can be widely used to investigate reactions when nuclear quantum effects and electronic nonadiabatic transitions play a dominant role in determining reaction mechanisms, such as condensed-phase and photoinduced PCET reactions.[3,7] Compared to the commonly used FSSH with vibronic-state representation,[7,68] RPSH avoids calculating a massive number of vibronic states for the proton yet provides accurate nuclear tunneling effects, thus making it possible to describe multiple proton transfer reactions. On the other hand, compared to the regular RPMD approach that treats an electron in its coordinate representation with the ring polymer quantization[5,69] and thus is limited to only one-electron nonadiabatic reactions,[42] RPSH can go beyond this limitation and describe multiple electron transfer reactions with the many-electron adiabatic representation.

Finally, this work will inspire engineering new approximated quantum dynamics methods that are capable of accounting for both electronic nonadiabatic transitions and nuclear quantum effects, just like RPSH. This proposal is summarized in Figure 5. With the methods along the *x*-axis, one can gradually increase the accuracy for describing electronic nonadiabatic effects. With the methods along the *y*-axis, one can gradually increase the accuracy for describing nuclear quantum effects. The purple shaded area indicates approximated methods that can capture both effects. More accurate but potentially numerically demanding methods can be engineered.

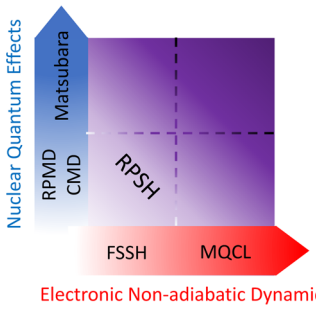

Figure 5. Schematic illustration of the route for developing new methods that incorporate nuclear and electronic quantum effects.

In summary, we applied the RPSH approach to investigate the real-time nonadiabatic dynamics with explicit nuclear quantum effects in Tully's Model systems. With explicit nuclear quantization through the ring polymer extended phase space description, we demonstrated that RPSH can properly describe tunneling, nuclear ZPE, and decoherence. By including the above essential physics, RPSH can provide more accurate nonadiabatic dynamics compared to FSSH. RPSH can be widely used to investigate photoinduced PCET reactions or nonadiabatic proton transfer reactions, where the interplay of quantum transitions and proton tunneling determines the reaction mechanism.

■ ASSOCIATED CONTENT

Supporting Information

The Supporting Information is available free of charge on the ACS Publications website at DOI: 10.1021/acs.jpclett.7b01343.

Hamiltonians and the corresponding parameters for Tully's Models I−III, additional results on using different initial conditions for FSSH and RPHS, an alternative velocity rescaling scheme based on ring polymer energy conservation with the corresponding numerical results, time-dependent electronic-state populations for Tully's Models I and II, and a three-state Morse potential (PDF)

■ AUTHOR INFORMATION

Corresponding Authors

*E-mail: farnaz.shakib@rochester.edu (F.A.S.).
*E-mail: pengfei.huo@rochester.edu (P.H.).

ORCID

Pengfei Huo: 0000-0002-8639-9299

Notes

The authors declare no competing financial interest.

■ ACKNOWLEDGMENTS

This work was supported by the University of Rochester startup funds. Computing resources were provided by the Center for Integrated Research Computing (CIRC) at the University of Rochester. We appreciate the TOC figure from Arkajit Mandal. F.A.S. appreciates valuable discussions with Drs. Philip Shushkov, Neil Shenvi, and Tim Hele. P.H. appreciates valuable discussions with Mr. Joonho Lee, Dr. Artur Menzeleev, and Prof. Tom Miller.

■ REFERENCES

(1) Huynh, M. H. V.; Meyer, T. G. Proton-Coupled Electron Transfer. *Chem. Rev.* **2007**, *107*, 5004−5064.
(2) Meyer, T. G.; Huynh, M. H. V.; Thorp, H. H. The Possible Role of Proton-Coupled Electron Transfer (PCET) in Water Oxidation by Photosystem II. *Angew. Chem., Int. Ed.* **2007**, *46*, 5284−5304.
(3) Hammes-Schiffer, S.; Stuchebrukhov, A. A. Theory of Coupled Electron and Proton Transfer Reactions. *Chem. Rev.* **2010**, *110*, 6939−6960.
(4) Weinberg, D. R.; Gagliardi, C. J.; Hull, J. F.; Murphy, C. F.; Kent, C. A.; Westlake, B. C.; Paul, A.; Ess, D. H.; McCafferty, D. G.; Meyer, T. J. Proton-Coupled Electron Transfer. *Chem. Rev.* **2012**, *112*, 4016−4093.
(5) Kretchmer, J. S.; Miller, T. F., III Direct simulation of proton-coupled electron transfer across multiple regimes. *J. Chem. Phys.* **2013**, *138*, 134109.
(6) Soudackov, A. V.; Hammes-Schiffer, S. Nonadiabatic Rate Constants for Proton Transfer and Proton-Coupled Electron Transfer Reactions in Solution: Effects of Quadratic Term in the Vibronic Coupling Expansion. *J. Chem. Phys.* **2015**, *143*, 194101.
(7) Goyal, P.; Schwerdtfeger, C. A.; Soudackov, A. V.; Hammes-Schiffer, S. Proton Quantization and Vibrational Relaxation in Nonadiabatic Dynamics of Photo Induced Proton-Coupled Electron Transfer. *J. Phys. Chem. B* **2016**, *120*, 2407−2417.
(8) Shakib, F. A.; Hanna, G. An Analysis of Model Proton-Coupled Electron Transfer Reactions via the Mixed Quantum-Classical Liouville Approach. *J. Chem. Phys.* **2014**, *141*, 044122.
(9) Shakib, F. A.; Hanna, G. New Insights into the Nonadiabatic State Population Dynamics of Model Proton-Coupled Electron

DOI: 10.1021/acs.jpclett.7b01343
J. Phys. Chem. Lett. 2017, 8, 3073−3080

Transfer Reactions from the Mixed Quantum-Classical Liouville Approach. *J. Chem. Phys.* **2016**, *144*, 024110.
(10) Ehrenfest, P. Bemerkung Über Die Angenäherte Gültigkeit Der Klassischen Mechanik Innerhalb Der Quantenmechanik. *Eur. Phys. J. A* **1927**, *45*, 455−457.
(11) Sawada, S.; Nitzan, A.; Metiu, H. Mean-Trajectory Approximation for Charge-Transfer and Energy-Transfer Processes at Surfaces. *Phys. Rev. B: Condens. Matter Mater. Phys.* **1985**, *32*, 851−867.
(12) Prezhdo, O. V.; Kisil, V. V. Mixing Quantum and Classical Mechanics. *Phys. Rev. A: At., Mol., Opt. Phys.* **1997**, *56*, 162−175.
(13) Tully, J. C. Molecular Dynamics with Electronic Transitions. *J. Chem. Phys.* **1990**, *93*, 1061−1071.
(14) Hammes-Schiffer, S.; Tully, J. C. Proton transfer in solution: Molecular dynamics with quantum transitions. *J. Chem. Phys.* **1994**, *101*, 4657−4667.
(15) Kapral, R.; Ciccotti, G. Mixed quantum classical dynamics. *J. Chem. Phys.* **1999**, *110*, 8919−8929.
(16) Kapral, R. Surface Hopping from the Perspective of Quantum-Classical Liouville Dynamics. *Chem. Phys.* **2016**, *481*, 77−83.
(17) Miller, W. H. The Semiclassical Initial Value Representation: A Potentially Practical Way for Adding Quantum Effects to Classical Molecular Dynamics Simulations. *J. Phys. Chem. A* **2001**, *105*, 2942−2955.
(18) Wang, H. B.; Sun, X.; Miller, W. H. Semiclassical Approximations for the Calculation of Thermal Rate Constants for Chemical Reactions in Complex Molecular Systems. *J. Chem. Phys.* **1998**, *108*, 9726−9736.
(19) Sun, X.; Wang, H. B.; Miller, W. H. Semiclassical Theory of Electronically Nonadiabatic Dynamics: Results of a Linearized Approximation to the Initial Value Representation. *J. Chem. Phys.* **1998**, *109*, 7064−7074.
(20) Shi, Q.; Geva, E. Nonradiative Electronic Relaxation Rate Constants from Approximations Based on Linearizing the Path-Integral Forward-Backward Action. *J. Phys. Chem. A* **2004**, *108*, 6109−6116.
(21) Sun, X.; Geva, E. Non-Condon nonequilibrium Fermi's golden rule rates from the linearized semiclassical method. *J. Chem. Phys.* **2016**, *145*, 064109/1−064109/19.
(22) Huo, P.; Coker, D. F. Communication: Partial linearized density matrix dynamics for dissipative, non-adiabatic quantum evolution. *J. Chem. Phys.* **2011**, *135*, 201101/1−201101/4.
(23) Huo, P.; Miller, T. F.; Coker, D. F. Communication: Predictive partial linearized path integral simulation of condensed phase electron transfer dynamics. *J. Chem. Phys.* **2013**, *139*, 151103/1−151103/4.
(24) Barbatti, M. Nonadiabatic Dynamics with Trajectory Surface Hopping Method. *Wiley Interdiscip. Rev. Comput. Mol. Sci.* **2011**, *1*, 620−633.
(25) Subotnik, J. E.; Jain, A.; Landry, B.; Petit, A.; Ouyang, W.; Bellonzi, N. Understanding the Surface Hopping View of Electronic Transitions and Decoherence. *Annu. Rev. Phys. Chem.* **2016**, *67*, 387−417.
(26) Wang, L.; Akimov, A. V.; Prezhdo, O. V. Recent Progress in Surface Hopping: 2011−2015. *J. Phys. Chem. Lett.* **2016**, *7*, 2100−2012.
(27) Prezhdo, O. V.; Rossky, P. J. Mean-field Molecular Dynamics with Surface Hopping. *J. Chem. Phys.* **1997**, *107*, 825−834.
(28) Topaler, M. S.; Allison, T. C.; Schwenke, D. W.; Truhlar, D. G. Test of Trajectory Surface Hopping Against Accurate Quantum Dynamics for an Electronically Nonadiabatic Chemical Reaction. *J. Phys. Chem. A* **1998**, *102*, 1666−1673.
(29) Hack, M. D.; Wensmann, A. M.; Truhlar, D. G.; Ben-Nun, M.; Martinez, T. J. Comparison of Full Multiple Spawning, Trajectory Surface Hopping, and Converged Quantum Mechanics for Electronically Nonadiabatic Dynamics. *J. Chem. Phys.* **2001**, *115*, 1172−1186.
(30) Fang, J. Y.; Hammes-Schiffer, S. Improvement of the Internal Consistency in Trajectory Surface Hopping. *J. Phys. Chem. A* **1999**, *103*, 9399−9407.
(31) Subotnik, J. E.; Shenvi, N. Decoherence and Surface Hopping: When Can Averaging Over Initial Conditions Help Capture the Effects of Wave Packet Separation? *J. Chem. Phys.* **2011**, *134*, 244114.
(32) Granucci, G.; Persico, M.; Zoccante, A. Including quantum decoherence in surface hopping. *J. Chem. Phys.* **2010**, *133*, 134111/1−134111/9.
(33) Shenvi, N.; Subotnik, J. E.; Yang, W. Simultaneous-Trajectory Surface Hopping: A Parameter-Free Algorithm for Implementing Decoherence in Nonadiabatic Dynamics. *J. Chem. Phys.* **2011**, *134*, 144102.
(34) Shenvi, N.; Subotnik, J. E.; Yang, W. Phase-Corrected Surface Hopping: Correcting the Phase Evolution of the Electronic Wavefunction. *J. Chem. Phys.* **2011**, *135*, 024101.
(35) Jaeger, H. M.; Fischer, S.; Prezhdo, O. V. Decoherence-Induced Surface Hopping. *J. Chem. Phys.* **2012**, *137*, 22A545−1.
(36) Akimov, A. V.; Prezhdo, O. V. Second-Quantized Surface Hopping. *Phys. Rev. Lett.* **2014**, *113*, 153003.
(37) Wang, L.; Sifain, A. E.; Prezhdo, O. V. Communication: Global Flux Surface Hopping in Liouville Space. *J. Chem. Phys.* **2015**, *143*, 191102.
(38) Wang, L. J.; Sifain, A. E.; Prezhdo, O. V. Fewest Switches Surface Hopping in Liouville Space. *J. Phys. Chem. Lett.* **2015**, *6*, 3827−3833.
(39) Cao, J.; Voth, G. A. The Formulation of Quantum Statistical Mechanics based on the Feynman Path Centroid Density. IV. Algorithms for Centroid Molecular Dynamics. *J. Chem. Phys.* **1994**, *101*, 6168−6183.
(40) Jang; Voth, G. A Derivation of Centroid Molecular Dynamics and Other Approximate Time Evolution Methods for Path Integral Centroid Variables. *J. Chem. Phys.* **1999**, *111*, 2371−2384.
(41) Craig, I. R.; Manolopoulos, D. E. Quantum Statistics and Classical Mechanics: Real Time Correlation Functions from Ring Polymer Molecular Dynamics. *J. Chem. Phys.* **2004**, *121*, 3368−3373.
(42) Habershon, S.; Manolopoulos, D. E.; Markland, T. E.; Miller, T. F. Ring-Polymer Molecular Dynamics: Quantum Effects in Chemical Dynamics from Classical Trajectories in an Extended Phase Space. *Annu. Rev. Phys. Chem.* **2013**, *64*, 387−413.
(43) Menzeleev, A. R.; Ananth, N.; Miller, T. F., III Direct Simulation of Electron Transfer Using Ring Polymer Molecular Dynamics: Comparison with Semiclassical Instanton Theory and Exact Quantum Methods. *J. Chem. Phys.* **2011**, *135*, 074106.
(44) Liao, J. L.; Voth, G. A. A Centroid Molecular Dynamics Approach for Nonadiabatic Dynamical Processes in Condensed Phases: The Spin-Boson Case. *J. Phys. Chem. B* **2002**, *106*, 8449−8455.
(45) Shushkov, P.; Li, R.; Tully, J. C. Ring Polymer Dynamics with Surface Hopping. *J. Chem. Phys.* **2012**, *137*, 22A549.
(46) Menzeleev, A. R.; Bell, F.; Miller, T. F., III Kinetically Constrained Ring-Polymer Molecular Dynamics for Non-Adiabatic Chemical Reactions. *J. Chem. Phys.* **2014**, *140*, 064103.
(47) Ananth, N. Mapping Variable Ring Polymer Molecular Dynamics: A Path-Integral Based Method for Nonadiabatic Processes. *J. Chem. Phys.* **2013**, *139*, 124102.
(48) Richardson, J. O.; Thoss, M. Communication: Nonadiabatic Ring-Polymer Molecular Dynamics. *J. Chem. Phys.* **2013**, *139*, 031102.
(49) Duke, J. R.; Ananth, N. Simulating Excited State Dynamics in Systems with Multiple Avoided Crossings Using Mapping Variable Ring Polymer Molecular Dynamics. *J. Phys. Chem. Lett.* **2015**, *6*, 4219−4223.
(50) Duke, J. R.; Ananth, N. Mean Field Ring Polymer Molecular Dynamics for Electronically Nonadiabatic Reaction Rates. *Faraday Discuss.* **2016**, *195*, 253−268.
(51) Lu, J.; Zhou, J. Path integral molecular dynamics with surface hopping for thermal equilibrium sampling of nonadiabatic systems. *J. Chem. Phys.* **2017**, *146*, 154110.
(52) Batista, V. S.; Coker, D. F. Nonadiabatic Molecular Dynamics Simulation of Photodissociation and Geminate Recombination of I2 Liquid Xenon. *J. Chem. Phys.* **1996**, *105*, 4033−4054.

DOI: 10.1021/acs.jpclett.7b01343
J. Phys. Chem. Lett. 2017, 8, 3073−3080

(53) Müller, U.; Stock, G. Surface-hopping modeling of photoinduced relaxation dynamics on coupled potential-energy surfaces. *J. Chem. Phys.* **1997**, *107*, 6230−6245.
(54) Agostini, F.; Min, S. K.; Abedi, A.; Gross, E. K. U. Quantum-Classical Nonadiabatic Dynamics: Coupled vs Independent-Trajectory Methods. *J. Chem. Theory Comput.* **2016**, *12*, 2127−2143.
(55) Morelli, J.; Hammes-Schiffer, S. Surface hopping and fully quantum dynamical wavepacket propagation on multiple coupled adiabatic potential surfaces for proton transfer reactions. *Chem. Phys. Lett.* **1997**, *269*, 161−170.
(56) Landry, B. R.; Subotnik, J. E. How to recover Marcus theory with fewest switches surface hopping: Add just a touch of decoherence. *J. Chem. Phys.* **2012**, *137*, 22A513/1−22A513/13.
(57) Vazquez, F. X.; Talapatra, S.; Geva, E. Vibrational Energy Relaxation in Liquid HCl and DCl via the Linearized Semiclassical Method: Electrostriction versus Quantum Delocalization. *J. Phys. Chem. A* **2011**, *115*, 9775−9781.
(58) Ma, Z.; Coker, D. F. Quantum initial condition sampling for linearized density matrix dynamics: Vibrational pure dephasing of iodine in krypton matrices. *J. Chem. Phys.* **2008**, *128*, 244108/1−244108/18.
(59) Poulsen, J. A.; Nyman, G.; Rossky, P. J. Quantum initial condition sampling for linearized density matrix dynamics: Vibrational pure dephasing of iodine in krypton matrices. *J. Chem. Phys.* **2003**, *119*, 12179−12193.
(60) Liu, J.; Miller, W. H. An Approach for Generating Trajectory-Based Dynamics which Conserves the Canonical Distribution in the Phase Space Formulation of Quantum Mechanics. I. *J. Chem. Phys.* **2011**, *134*, 104101/1−104101/14.
(61) Habershon, S.; Manolopoulos, D. E. Zero Point Energy Leakage in Condensed Phase Dynamics: An Assessment of Quantum Simulation Methods for Liquid Water. *J. Chem. Phys.* **2009**, *131*, 244518.
(62) Collepardo-Guevara, R.; Craig, I. R.; Manolopoulos, D. E. Proton transfer in a polar solvent from ring polymer reaction rate theory. *J. Chem. Phys.* **2008**, *128*, 144502/1−144502/13.
(63) Craig, I. R.; Manolopoulos, D. E. Chemical reaction rates from ring polymer molecular dynamics. *J. Chem. Phys.* **2005**, *122*, 084106/1−084106/12.
(64) Hele, T. J. H.; Willatt, M. J.; Muolo, A.; Althorpe, S. C. Communication: Relation of Centroid Molecular Dynamics and Ring-Polymer Molecular Dynamics to Exact Quantum Dynamics. *J. Chem. Phys.* **2015**, *142*, 191101.
(65) Hele, T. J. H.; Willatt, M. J.; Muolo, A.; Althorpe, S. C. Boltzmann-Conserving Classical Dynamics in Quantum Time-Correlation Functions: "Matsubara Dynamics". *J. Chem. Phys.* **2015**, *142*, 134103.
(66) Subotnik, J. E.; Ouyang, W.; Landry, B. R. Can We Derive Tully's Surface-Hopping Algorithm from the Semiclassical Quantum Liouville Equation? Almost, But Only with Decoherence. *J. Chem. Phys.* **2013**, *139*, 214107.
(67) Hele, T. J. H.; Ananth, N. Deriving the Exact Nonadiabatic Quantum Propagator in the Mapping Variable Representation. *Faraday Discuss.* **2016**, *195*, 269−289.
(68) Hazra, A.; Soudackov, A. V.; Hammes-Schiffer, S. Role of Solvent Dynamics in Ultrafast Photoinduced Proton-Coupled Electron Transfer Reactions in Solution. *J. Phys. Chem. B* **2010**, *114*, 12319−12332.
(69) Kretchmer, J. S.; Miller, T. F., III Tipping the balance between concerted versus sequential proton-coupled electron transfer. *Inorg. Chem.* **2016**, *55*, 1022−1031.

DOI: 10.1021/acs.jpclett.7b01343
J. Phys. Chem. Lett. 2017, 8, 3073−3080